

---

# Predicting mutational effects on protein binding from folding energy

---

Arthur Deng<sup>1</sup> Karsten Householder<sup>1</sup> Fang Wu<sup>1</sup> K. Christopher Garcia<sup>1</sup> Brian Trippe<sup>1</sup>

## Abstract

Accurate estimation of mutational effects on protein-protein binding energies is an open problem with applications in structural biology and therapeutic design. Several deep learning predictors for this task have been proposed but, presumably due to the scarcity of binding data, these methods under-perform computationally expensive estimates based on empirical force-fields. In response, we propose a transfer-learning approach that leverages advances in protein sequence modeling and folding stability prediction for this task. The key idea is to parameterize the binding energy as the difference between the folding energy of the protein complex and the sum of the folding energies of its binding partners. We show that using a pre-trained inverse-folding model as a proxy for folding energy provides strong zero-shot performance, and can be fine-tuned with (1) copious folding energy measurements and (2) more limited binding energy measurements. The resulting predictor, STAB-DDG, is the first deep learning predictor to match the accuracy of the state-of-the-art empirical force-field method Flex ddG, while offering an over 10,000x speed-up.

## 1. Introduction

Computation of mutational effects on binding energies is of central importance in structural biology and protein engineering. For example, three recent studies (Householder et al., 2024; Liu et al., 2024a; Johansen et al., 2024) designed proteins that bind to target proteins found on cancer cells, but the therapeutic promise of these molecules depends on their specificity; “off-target” binding to proteins differing at only one or two positions could induce toxicity to non-cancer cells (see Appendix A). In this setting and others, accurate prediction of binding energies would sup-

port *in silico* design of proteins with requisite specificity. Given two interacting proteins and amino acid substitutions, the goal is to predict the differences in the change in Gibbs free energy upon binding (the “ $\Delta\Delta G$ ” or “ddG”).

Despite enormous progress provided by deep-learning (DL) methods on a variety of protein modeling and design problems (Dauparas et al., 2022; Watson et al., 2023; Abramson et al., 2024; Dieckhaus et al., 2024), they have so far underperformed more classical methods based on empirical force-fields on binding energy prediction. Notably, Bushuiev et al. (2024) find that recent results suggesting the superiority of DL predictors are confounded by dataset contamination — extant DL predictors generalize poorly when evaluated on interfaces not represented in the training set, and a Rosetta-based predictor Flex ddG provides state-of-the-art performance (Barlow et al., 2018; Bushuiev et al., 2024). Presumably, this underperformance of DL methods owes in part to the scarcity of experimental  $\Delta\Delta G$  measurements used to fit such models, with binding interaction measurements for fewer than 350 distinct interfaces in the largest public curated dataset (Jankauskaitė et al., 2019).

In this work, we introduce a transfer learning approach that helps address this data limitation by reducing binding energy prediction to predicting folding energies. Our approach is based on two observations. First, as a consequence of the state function property of free energy, the binding energy between two proteins  $A$  and  $B$ ,  $\Delta G_{\text{bind}}(A:B)$ , can be computed as

$$\Delta G_{\text{bind}}(A:B) = \Delta G_{\text{fold}}(A:B) - \Delta G_{\text{fold}}(A) - \Delta G_{\text{fold}}(B), \quad (1)$$

where  $\Delta G_{\text{fold}}$  denotes the free energy difference between *folded* and *unfolded* states of a protein monomer or complex (Figure 1a). This observation will allow us to use both folding stability and binding energy datasets in a supervised learning approach.

The second observation is that protein sequences and structure data in the Protein Data Bank (PDB) can inform an initial predictor of protein folding energies. This observation builds on the strong correlation between folding energies and likelihoods predicted by probabilistic models of protein sequences. Such correlations were first observed for Potts models (Lapedes et al., 2012; Hopf et al., 2017), and then later neural network models of sequence (Riesselman et al.,

---

<sup>1</sup>Stanford University. Correspondence to: Arthur Deng <lx-deng@stanford.edu>, Brian Trippe <btrippe@stanford.edu>.

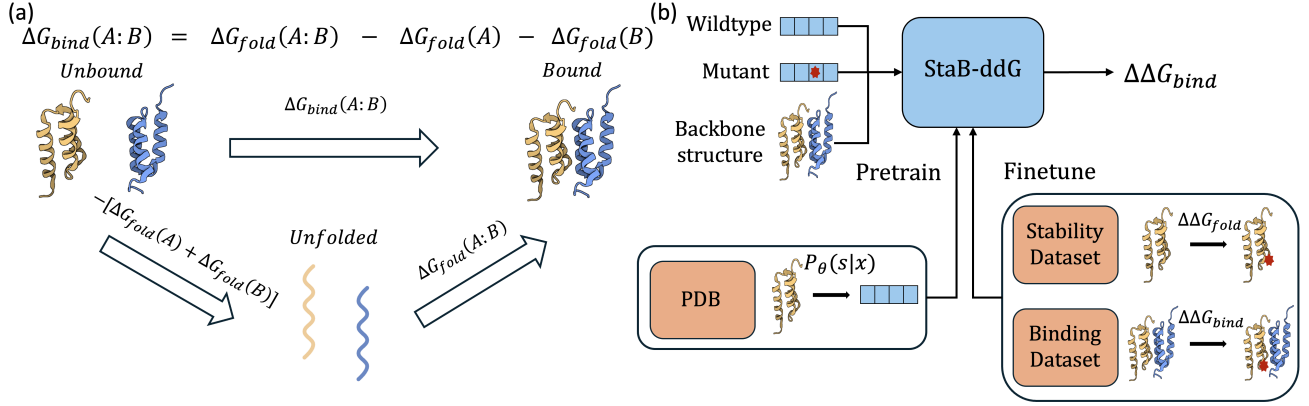


Figure 1. (a) Thermodynamic identity from the path independence of the free energy function (Equation (1)). (b) Schematic of STAB-DDG. STAB-DDG takes as input the backbone structure, a wild type sequence, and a mutant sequence to predict  $\Delta \Delta G_{\text{bind}}$ . STAB-DDG leverages three sources of data: structure/sequence pairs from the PDB, a folding stability dataset, and a binding affinity dataset.

2018; Rives et al., 2021), as well as backbone structure conditional sequence models (Hsu et al., 2022a; Notin et al., 2023). We can leverage these correlations by using a pre-trained sequence likelihood model as a zero-shot folding energy predictor.

Built on these observations, we present **Stability-to-Binding delta delta G** (STAB-DDG), a deep learning model to predict the mutation effects on protein-protein interaction energy using interface structure and sequence (Figure 1b). To fit STAB-DDG, we use a pre-trained inverse folding model ProteinMPNN (Dauparas et al., 2022) to initialize a zero-shot binding  $\Delta \Delta G$  predictor according to Equation (1), and fine-tune on a combination of high-throughput folding energy measurements (Tsuboyama et al., 2023) and binding energy measurements (Jankauskaitė et al., 2019).

We demonstrate that fine-tuning STAB-DDG on a folding energy dataset improves binding energy predictions. Further fine-tuning on binding energy data provides state-of-the-art performance on a standard benchmark. Lastly, we evaluate STAB-DDG on two difficult case study datasets that corroborate these conclusions but illustrate that the problem remains difficult.

## 2. Preliminaries

In this section, we outline relevant background on protein thermodynamics and describe the notation used.

**Protein binding, folding, and mutational effects.** The binding energy between two proteins  $A$  and  $B$  is the free energy difference,  $\Delta G_{\text{bind}}(A:B)$ , between the *bound* and *unbound* (but folded) states of the system. Our goal is to predict the effect of mutations on binding energies. For a reference (wild type) interaction  $A:B$  and mutant  $A':B$ ,

we write the mutational effect as

$$\Delta \Delta G_{\text{bind}}(A:B \rightarrow A':B) = \Delta G_{\text{bind}}(A':B) - \Delta G_{\text{bind}}(A:B).$$

Our starting point is the observation in Equation (1) that  $\Delta G_{\text{bind}}$  may be computed as a difference in folding stabilities  $\Delta G_{\text{fold}}$  as a consequence of the state function property of free energies; the change in energy along a direct path from the unbound to bound states is the same as the change along the path that proceeds through the unfolded state (Figure 1a).

Using Equation (1), we can express  $\Delta \Delta G_{\text{bind}}$  in terms of folding energy as

$$\Delta \Delta G_{\text{bind}}(A:B \rightarrow A':B) = \Delta \Delta G_{\text{fold}}(A:B \rightarrow A':B) - \Delta \Delta G_{\text{fold}}(A \rightarrow A'). \quad (2)$$

Equation (2) underlies binding  $\Delta \Delta G$  predictors based on empirical force fields (e.g., Kastiris & Bonvin, 2013; Barlow et al., 2018). But to our knowledge this identity has not previously been leveraged in a DL binding  $\Delta \Delta G$  predictor.

**Notation.** We represent a protein by its amino acid sequence  $s = [s^1, s^2, \dots, s^L]$  where  $L$  is the length of the sequence and each  $s^l \in \{1, \dots, 20\}$  indicates the amino acid type. For binding partners  $A$  and  $B$ , we write  $s_{A:B} = (s_A, s_B)$  to denote the protein complex. Mutations of sequences  $s$  are written as  $s'$  and are assumed to be of the same length.

## 3. Predicting mutational effects on protein binding from folding energy

To incorporate labeled fine-tuning data with a pre-trained sequence likelihood model, we first propose STAB-DDG, a

binding energy predictor based on sequence log probability. We show that STAB-DDG satisfies three properties we argue are desirable of  $\Delta\Delta G$  predictors but that are not satisfied by previous predictors. Then, we present an objective to fine-tune STAB-DDG on both folding stability and binding affinity datasets. Lastly, we discuss variance reduction techniques to reduce prediction error at both training and inference time.

### 3.1. The STAB-DDG predictor

To obtain a binding  $\Delta\Delta G$  predictor we start with a pre-trained sequence likelihood model to initialize a protein stability ( $\Delta G_{\text{fold}}$ ) predictor as

$$f_{\theta}(s) = \log p_{\theta}(s), \quad (3)$$

Where  $p_{\theta}(s)$  is a probability model on sequences. We take the logarithm of  $p_{\theta}$  to agree with the close-to-linear relationship between log probabilities of protein sequences and folding energies observed by [Lapedes et al. \(2012\)](#) and corroborated by many others ([Notin et al., 2023](#)). We use the ProteinMPNN inverse-folding model ([Dauparas et al., 2022](#)) for  $f_{\theta}(s)$ . ProteinMPNN depends additionally on a reference backbone structure but we leave this dependence implicit to simplify notation.

Then, using Equation 1, we can obtain a binding affinity ( $\Delta G_{\text{bind}}(A : B)$ ) predictor as

$$b_{\theta}(s_{A:B}) = f_{\theta}(s_{A:B}) - f_{\theta}(s_A) - f_{\theta}(s_B). \quad (4)$$

We refer to Equation (4) as the StaB parameterization because it links a **Stability** to **Binding**. Finally, we can use a difference of the predicted binding affinity between two complexes as a  $\Delta\Delta G_{\text{bind}}$  predictor as

$$\Delta b_{\theta}(s, s') = b_{\theta}(s') - b_{\theta}(s). \quad (5)$$

We call the predictors with the form  $\Delta b_{\theta}$  STAB-DDG predictors.

Computation of  $\Delta b_{\theta}(s, s')$  involves computing  $f_{\theta}$  on up to six systems; the complex and two binding partners for each of  $s$  and  $s'$ . While in principle the backbone structures for each term could vary, we use backbone structures derived from a single complex for all 6 terms. This choice reflects an assumption that the backbone changes little upon binding and mutation.

**The choice of ProteinMPNN.** We choose ProteinMPNN to initialize  $f_{\theta}$  and by extension  $b_{\theta}$  and  $\Delta b_{\theta}$ . ProteinMPNN offers two advantages over sensible alternatives. First, compared to (even much larger) protein language models that do not take as input a reference backbone structure, ProteinMPNN provides stronger zero-shot folding stability predictions ([Notin et al., 2023](#)). This fact presumably owes to that

mutational effects on binding are mediated through effects on structure.

The second advantage is that ProteinMPNN can make predictions for multi-chain complexes and multiple mutations. By contrast, most other folding stability predictors are implemented only for monomers and single mutations ([Dieckhaus et al., 2024](#); [Diaz et al., 2024](#)). This complication, though likely surmountable with heuristics such as glycine linkers or residue gaps, is avoided with ProteinMPNN.

**Properties of the StaB-ddG predictor.** The form of  $\Delta b_{\theta}$  constructed in Equations (3) to (5) imparts properties desirable of a  $\Delta\Delta G_{\text{bind}}$  predictor. We formalize these properties in the following proposition.

**Proposition 3.1.** *Consider the class of binding energy predictors  $\mathcal{B} = \{\Delta b_{\theta}\}$ , with  $\Delta b_{\theta}$  parameterized as in Equation (5) by  $p_{\theta}(s)$  that is an arbitrary  $20^L$ -simplex valued function of  $s$ . The family of predictors  $\mathcal{B}$  satisfies*

1. *Antisymmetry: for any  $\Delta b_{\theta}$  in  $\mathcal{B}$ ,*

$$\Delta b_{\theta}(s, s') = -\Delta b_{\theta}(s', s),$$

2. *Mutational path independence: for any  $\Delta b_{\theta}$  in  $\mathcal{B}$  and  $s, s', s''$ ,*

$$\Delta b_{\theta}(s, s') = \Delta b_{\theta}(s, s'') + \Delta b_{\theta}(s'', s'), \text{ and}$$

3. *Expressivity (Informal): for any dataset of binding free energy measurements, there exists a  $\Delta b_{\theta}$  in  $\mathcal{B}$  that fits the measurements exactly.*

*Proof:* Properties 1 and 2 follow immediately from the construction of  $\Delta b_{\theta}$  as the difference of evaluations of  $b_{\theta}$  defined in Equation (5). Appendix B provides a formal statement of the expressivity property along with a proof.

Because  $\Delta\Delta G_{\text{bind}}$ 's are differences by definition, they necessarily satisfy Properties 1 and 2 of Proposition 3.1. Though these properties are readily obtained in our predictor by construction, they are nonetheless not satisfied by other recent DL predictors (Table 1).

Property 3 requires  $p_{\theta}(s)$  to be able to take arbitrary values on the simplex. In practice,  $p_{\theta}(\cdot)$  is parametrized by ProteinMPNN which, as an auto-regressive model parameterized by a deep message-passing neural network, can approximate to arbitrary simplex-valued functions. This property formalizes the ability of our predictor to model epistasis and achieve zero training loss on the fine-tuning dataset. In contrast, a predictor parameterized by a masked language model (e.g., [Bushuiev et al., 2024](#)) cannot model non-additive effects between multiple mutations (Appendix B) and force field-based methods (e.g., Flex ddG) do not have this property.

Table 1. Thermodynamic properties of different  $\Delta\Delta G$  predictors. See Appendix B for detail.

Predictor	Anti-symmetry	Mut. Path Independence	Expressivity
Flex ddG	✓	✓	×
Surface-VQMAE	×	×	✓
Prompt-DDG	×	×	✓
DiffAffinity	×	×	✓
ProMIM	×	×	✓
RDE-Net	✓	×	✓
PPIformer	✓	×	×
STAB-DDG	✓	✓	✓

### 3.2. Assimilation of folding and binding energy data

Though our goal is to predict binding, the number of binding energy measurements available in the largest public curated set is two orders of magnitude fewer than that in the largest comparable set of folding stability measurements (Table 2). As such, we adopt a sequential fine-tuning strategy, where we first fine-tune on folding stability data and then fine-tune on more limited binding affinity data.

Table 2. Dataset size comparison between PDB and the largest available stability and binding datasets.

DATASET	# OF STRUCTURES	# OF MEASURED $\Delta\Delta G$
PDB	230,744	—
STABILITY	412	776,298
BINDING	345	7,085

**Fine-tuning to folding stability data.** The Megascala stability dataset is the largest publicly available dataset on protein folding energy with 776,298 folding stability measurements across 412 small monomeric proteins from a high throughput assay (Tsuboyama et al., 2023). We follow the same dataset preparation protocol as described by Dieckhaus et al. (2024), but keep entries with multiple mutations. We represent the Megascala stability dataset with  $N$  structures and  $M_n$  mutants associated with the  $n$ th structure as

$$\mathcal{D}_{\text{fold}} = \{(x_n, s_{n,\text{ref}}, y_{n,\text{ref}}, \{s_{n,m}, y_{n,m}\}_{m=1}^{M_n})\}_{n=1}^N,$$

where  $s_{n,\text{ref}}$  and  $y_{n,\text{ref}}$  denote the reference sequence and  $\Delta G$ , and  $x_n$  is a predicted reference structure. We use  $\{s_{n,m}, y_{n,m}\}_{m=1}^{M_n}$  to denote the a set of mutant sequences and corresponding mutant  $\Delta G$  values. A set of  $\Delta\Delta G$  values can then be computed by taking the difference between mutant and reference  $\Delta G$ .

To fine-tune  $\theta$  on  $\mathcal{D}_{\text{fold}}$ , we construct a  $\Delta\Delta G_{\text{fold}}$  predictor as

$$\Delta f_{\theta}(s, s') = f_{\theta}(s') - f_{\theta}(s), \quad (6)$$

where we use the same structure  $x_n$  to compute  $f_{\theta}(s')$  and  $f_{\theta}(s)$ . Then, we fine-tune by minimizing

$$L_{\text{fold}}(\theta, \mathcal{D}_{\text{fold}}) = \frac{1}{N} \sum_n \frac{1}{M_n} \sum_m (\Delta f_{\theta}(s_{n,\text{ref}}, s_{n,m}) - (y_{n,m} - y_{n,\text{ref}}))^2, \quad (7)$$

where the  $\frac{1}{M_n}$  scaling ensures that each complex has equal contribution to the loss.

**Fine-tuning to binding affinity data.** We use SKEMPIv2.0, the largest publicly available binding affinity dataset with 7,085 binding  $\Delta\Delta G$  measurements across 345 complexes, for fine-tuning STAB-DDG and comparing it against other baseline methods (Jankauskaitė et al., 2019). SKEMPIv2.0 contains errors from the manual curation process, such as mislabelled entries or entries with different  $\Delta\Delta G$  values for the same mutation. Here, we apply a filtering procedure to the dataset based on one applied to SKEMPIv1.0 from previous work (Dourado & Flores, 2014; Barlow et al., 2018). Further, conducting comparisons on SKEMPIv2.0 fairly requires careful consideration. Bushuiev et al. (2024) pointed out data leakage based on homology in previous train/test splits of the dataset. However, the held-out test set used by Bushuiev et al. (2024) only contained five interface clusters. To address these problems, we divide the dataset based on the annotated structurally homologous clusters and apply a random train/test split, with 121 complexes in the fine-tuning dataset and 80 complexes in the held-out test split. The filtering and splitting procedure is fully described in Appendix C.

Analogously to the Megascala stability dataset, SKEMPIv2.0 can be instantiated as

$$\mathcal{D}_{\text{bind}} = \{(x_n, s_{n,\text{ref}}, y_{n,\text{ref}}, \{s_{n,m}, y_{n,m}\}_{m=1}^{M_n})\}_{n=1}^N$$

with the difference being  $y_{\text{ref},n}$  and  $y_{n,m}$  referring to binding  $\Delta G$  instead of folding  $\Delta G$  and  $x_n$  representing crystal structures instead of predicted structures. We fine-tune on these data by minimizing

$$L_{\text{fold}}(\theta, \mathcal{D}_{\text{bind}}) = \frac{1}{N} \sum_n \frac{1}{M_n} \sum_m (\Delta b_{\theta}(s_{n,\text{ref}}, s_{n,m}) - (y_{n,m} - y_{n,\text{ref}}))^2. \quad (8)$$

### 3.3. Variance reduction by Monte Carlo ensembling and antithetic variates

The choice to use ProteinMPNN as our parameterization of  $f_{\theta}(s)$  introduces model-specific stochasticity in the form of



a randomized decoding order and Gaussian noise to backbone coordinates. This stochasticity introduces variance that contributes to the prediction error.

We make explicit the dependence of the model output on the stochasticity as  $b_\theta(s|\epsilon)$  for a random variable  $\epsilon$ . Then, for two sequences  $s$  and  $s'$ , and a measurement  $y = \Delta\Delta G_{\text{bind}}$ , we can decompose the expected prediction error into contributions from squared bias and variance (see e.g., [Hastie et al., 2009](#), Chapter 7) as

$$\mathbb{E}[(b_\theta(s'|\epsilon') - b_\theta(s|\epsilon) - y)^2] = \underbrace{(\mathbb{E}[b_\theta(s'|\epsilon') - b_\theta(s|\epsilon)] - y)^2}_{\text{Bias}} + \underbrace{\text{Var}[b_\theta(s'|\epsilon') - b_\theta(s|\epsilon)]}_{\text{Variance}},$$

where the randomness is taken over the stochasticity  $\epsilon$  and  $\epsilon'$ . We reduce the variance in two ways.

**Antithetic variates.** The first way is an instance of the antithetic variates method ([Hammersley & Morton, 1956](#)). The key idea is that the decomposition

$$\text{Var}[b_\theta(s'|\epsilon') - b_\theta(s|\epsilon)] = \text{Var}[b_\theta(s'|\epsilon')] + \text{Var}[b_\theta(s|\epsilon)] - 2\text{Cov}[b_\theta(s|\epsilon), b_\theta(s'|\epsilon')]$$

reveals that the correlation of  $b_\theta(s|\epsilon)$  with  $b_\theta(s'|\epsilon')$  decreases the overall variance. So any coupling of  $\epsilon$  and  $\epsilon'$  for which  $\text{Cov}[b_\theta(s|\epsilon), b_\theta(s'|\epsilon')]$  is positive will lead to lower variance than if  $\epsilon$  and  $\epsilon'$  were sampled independently. We accomplish this by fixing  $\epsilon' = \epsilon$ , which we implement by using the same permutation order and backbone noise for the wild type and mutant systems for each  $\Delta\Delta G$  prediction.

**Monte Carlo averaging.** The second way is Monte Carlo averaging. By replacing each prediction with its average across  $M$  independently sampled permutation orders and backbone noise samples, the variance is reduced by a factor of  $M$ . Ensembling can be applied together with the antithetic variates method by fixing  $\epsilon' = \epsilon$ . Note that ensembling over more samples increases the compute cost. We discuss the effects of ensemble size in Section 5.

## 4. Related work on predicting mutational effects on binding affinity

Existing approaches for predicting mutation effects on binding  $\Delta\Delta G$  can be categorized as empirical force field-based methods and DL-based. Force field-based methods use energy functions to model inter-atomic interactions ([Schymkowitz et al., 2005](#); [Park et al., 2016](#); [Barlow et al., 2018](#); [Sampson et al., 2024](#)). While these methods have long dominated the field, they are often computationally expensive and have limited accuracy. For example Flex ddG ([Barlow et al., 2018](#)) — a Rosetta-based predictor that is frequently considered to be state of the art in its

category ([Bushuiev et al., 2024](#)) — requires multiple CPU-hours per mutation but typically produces estimates with Pearson correlation to experimental  $\Delta\Delta G$ s no larger than  $R \approx 0.65$  ([Barlow et al., 2018](#)).

Free-energy perturbation (FEP) defines a class of potentially more accurate methods for estimating mutational effects ([Zwanzig, 1954](#)). Recent studies using FEP ([Sergeeva et al., 2023](#); [Abramson et al., 2024](#)) demonstrate small improvements over Flex ddG and related methods. However, these studies rely on a closed-source software implementation, case-specific expert tuning, and are even more computationally expensive. Consequently, we are unable to meaningfully assess accuracy of FEP methods.

Much recent work on  $\Delta\Delta G$  prediction methodology has focused DL approaches ([Luo et al., 2023](#); [Liu et al., 2024b](#); [Mo et al., 2024](#); [Bushuiev et al., 2024](#); [Wu & Li, 2024](#); [Wu et al., 2024](#)). None of these approaches incorporate folding stability data.

[Jiao et al. \(2024\)](#) propose an approach that decomposes the  $\Delta\Delta G$  computation into computing mutational effects in bound and unbound states, resulting in a ProteinMPNN-based predictor of the same form as STAB-DDG (but without our variance reduction techniques). However, they do not consider binding energy in terms of folding energy.

Several prior works on DL methods ([Luo et al., 2023](#); [Liu et al., 2024b](#); [Mo et al., 2024](#); [Bushuiev et al., 2024](#); [Wu & Li, 2024](#); [Wu et al., 2024](#)) have claimed to deliver performance surpassing force field-based predictors (e.g., Flex ddG) on the basis of performance on the SKEMPIv2.0 ([Jankauskaitė et al., 2019](#)) benchmark dataset. However, [Bushuiev et al. \(2024\)](#) find that the train/test splits used to support these claims suffer data leakage; once this data-leakage is corrected the performances of these deep learning predictors lag Flex ddG.

## 5. Experiments

To evaluate STAB-DDG we first analyze the contributions of different techniques that lead to an improvement in “zero-shot”  $\Delta\Delta G_{\text{bind}}$  prediction accuracy, without training on  $\Delta\Delta G_{\text{bind}}$  data. Next, we introduce baseline methods and show that STAB-DDG is the only DL approach to match Flex ddG. Finally, we assess the out-of-distribution accuracy of our approach by testing it on a yeast surface display binding dataset and a T cell receptor (TCR) mimic binding dataset that we curate.

In protein engineering applications, a  $\Delta\Delta G_{\text{bind}}$  prediction may be used to rank candidate sequence variants of an interface of interest to select as subset for experimental screening. Therefore, we compute Spearman’s rank correlation coefficient for mutational effects and predictions for each

interface, and report the mean of this metric across complexes, along with standard errors. We refer to this metric as “per interface Spearman”. When we compute per interface Spearman, we consider only complexes with 10 or more mutants; below this threshold, this metric suffers high variance (Appendix C).

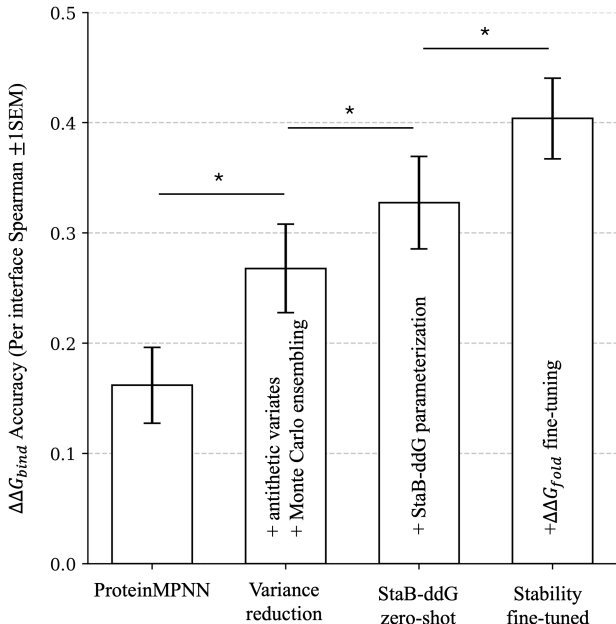


Figure 2. Evaluation of zero-shot binding predictors on the binding data training split. ProteinMPNN refers to using log-likelihoods of entire complexes ( $\Delta f_\theta$ ) from the pre-trained ProteinMPNN weights. Asterisks (\*) denote significance (one-sided paired t-test) at  $p < 0.05$ .

### 5.1. Contributions to zero-shot $\Delta\Delta G_{\text{bind}}$ accuracy.

We first examined the individual contributions of techniques from our method that, starting from ProteinMPNN, lead to a zero-shot binding energy predictor that incorporates information from folding stability data (Figure 2). We evaluated the binding energy prediction accuracy of different zero-shot predictors on the binding data training split described in Section 3.2.

**Variance reduction.** To reduce the error from the stochasticity inherent to ProteinMPNN, we applied the variance reduction techniques described in Section 3.3 and observed improved accuracy. Specifically, reducing the variance of the ProteinMPNN predictor by (1) fixing the decoding order and backbone noise between the wild type and mutant sequences, and (2) ensembling over 20 predictions significantly improved zero-shot performance (Figure 2). We found that fixing the decoding order and backbone noise also led to better training dynamics, and provide empirical validation for the choice of ensemble size in Appendix D.

**STAB-DDG zero-shot.** We applied the pre-trained weights with variance reduction in the form of the binding predictor  $\Delta b_\theta(s, s')$ . The resulting predictor, STAB-DDG zero-shot, uses the same weights as ProteinMPNN but achieved significantly better accuracy (Figure 2).

**Fine-tuning on folding stability data.** To validate whether fine-tuning on additional folding stability data translates to improved binding energy prediction accuracy, we fine-tuned STAB-DDG zero-shot on the folding stability dataset (“Stability fine-tuned”). We found that including these data further increased binding prediction accuracy (Figure 2). A question that arises is whether the large amount of folding stability data removes the need for unsupervised pre-training. We found that training directly on the folding stability dataset without inverse folding pre-training led to significantly worse binding prediction accuracy (Appendix D). This result highlights the importance of pre-training on a much more abundant and diverse set of structures from the PDB.

We validated our approach of fine-tuning on folding stability data of Tsuboyama et al. (2023) by comparing to a state-of-the-art folding stability predictor ThermoMPNN (Dieckhaus et al., 2024). ThermoMPNN is also based on ProteinMPNN but adds an additional transfer-learning module to output predictions. We found that despite not introducing additional parameters to ProteinMPNN, our stability fine-tuned model achieved performance not much lower than ThermoMPNN; our predictor provided a Spearman (over all domains) of 0.69 vs. 0.73 for ThermoMPNN (Appendix E).

We additionally explored different forms of the predictor and training techniques that did not have a sizeable effect. First, we tried fitting amino acid-specific offsets to the predictor in the form of a linear model to correct for the initial scale mismatch between sequence log-likelihoods and free energy, measured in kilocalories per mole. However adding these terms did not have a significant effect on binding prediction accuracy (Appendix D). Second, we experimented with using AlphaFold3 (Abramson et al., 2024) predicted structures to more accurately model the unbound (apo) structures of individual binders, instead of using the structure of the bound conformation. While using predicted apo structures improved several other metrics, this modification did not improve the per interface Spearman (Appendix D).

### 5.2. Comparison to existing methods

Using Stability fine-tuned as a starting point, we further fine-tuned this model on the binding data train split described in Section 3.2. We call the resulting predictor STAB-DDG.

We compared STAB-DDG to baseline methods on the binding data test split. Figure 3 presents per interface Spearman. We find similar trends for other metrics considered in pre-

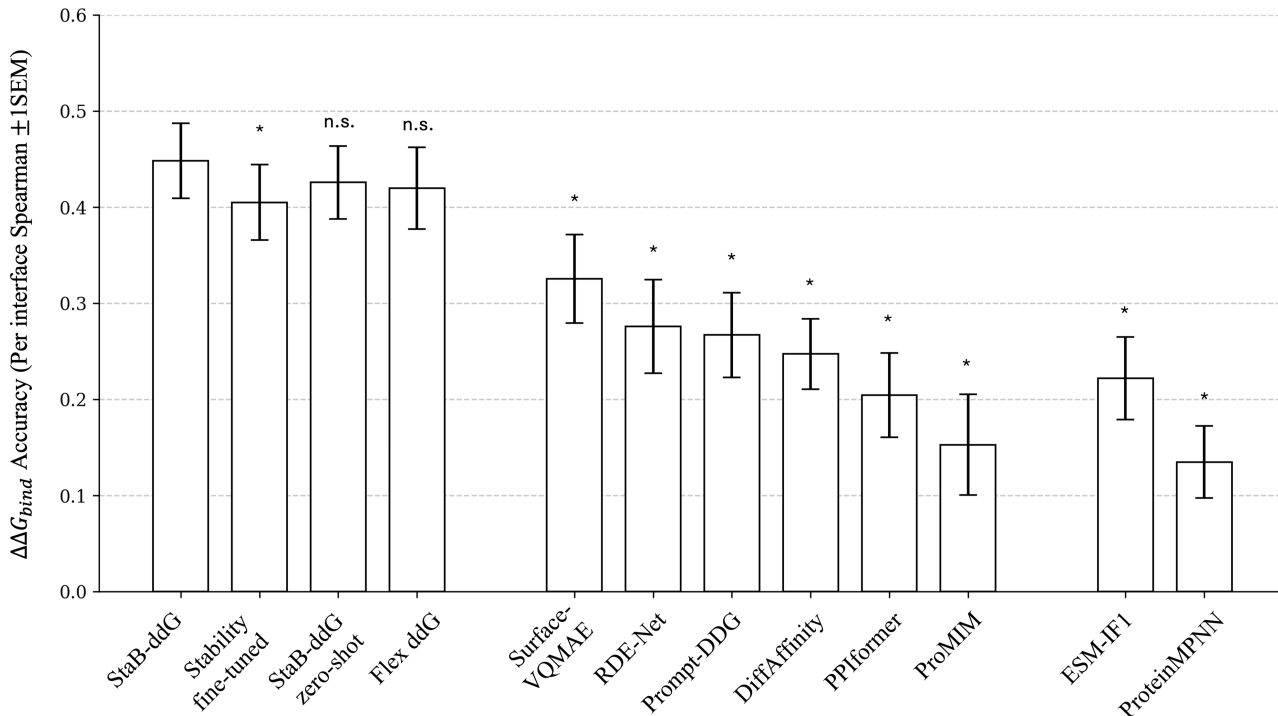


Figure 3. Evaluation of accuracy on the binding  $\Delta\Delta G_{\text{bind}}$  benchmark test split of SKEMPIv2. Left: STAB-DDG and its variations. Middle: Previous deep learning methods. Right: Inverse Folding models. \*: significance (one-sided paired t-test with STAB-DDG) at  $p < 0.05$ , n.s.: not significant.

vious works (Appendix E). We describe the baselines and then results.

**Baselines.** Flex ddG is a state-of-the-art force field simulation method based on the Rosetta energy function. It is an ML method owing to a key component being the reweighting the terms of the empirical energy function through a Generalized Additive Model (GAM) fitted onto the SKEMPIv1.0 dataset. It is possible that the overlap between the data used to fit the GAM and our test split can lead to inflated performance metrics for Flex ddG. Barlow et al. (2018) showed that backrub sampling, despite its high computational cost, is critical to the success of Flex ddG. While prior efforts to benchmark Flex ddG omit the backrub sampling steps to reduce computational cost (e.g., Bushuiev et al., 2024), we ran Flex ddG with the default parameters determined by Barlow et al. (2018), with the exception of setting the number of models to 10, a number shown to be near-optimal.

We compared to six supervised DL baselines, which we re-trained on our train/test split. All six DL baselines leverage pre-training on a larger unsupervised dataset before fine-tuning on binding energy data. We did not compare to Boltzmann Alignment (Jiao et al., 2024) as the parametric form of the predictor is similar to STAB-DDG zero-shot.

We included inverse-folding models ESM-IF1 and ProteinMPNN as unsupervised baselines (Dauparas et al., 2022; Hsu et al., 2022b). Zero-shot predictions were computed by subtracting the wild type complex sequence log-likelihood from the mutant log-likelihood.

**Results.** When evaluated on the binding data test split, STAB-DDG achieved the highest per structure Spearman (0.45), outperforming previous DL methods (Figure 3). Similar to Bushuiev et al. (2024), we found that the DL baselines underperform Flex ddG when evaluated on an interface homology-based split. We found STAB-DDG zero-shot to be surprisingly competitive, also outperforming previous DL methods, despite using the same model weights as ProteinMPNN. However, we did not find the difference between STAB-DDG, STAB-DDG zero-shot, and Flex ddG to be statistically significant based on a one-sided t-test. In addition, we found that the stability fine-tuned model achieved worse performance on the test split, highlighting the performance fluctuations owing to stochasticity from the random splits, motivating additional validation on other datasets.

**Experimental details.** In summary, we fine-tuned on the Megascap stability dataset using the ADAM optimizer with learning rate  $3e-5$  for 70 epochs with a batch size of 25,000 amino acids. We fine-tuned on SKEMPIv2.0 using the

ADAM optimizer with learning rate  $1e-6$  for 200 epochs with a batch size of 25,000 amino acids. We release our implementation of the method publicly<sup>1</sup>.

**Running time.** STAB-DDG is multiple orders of magnitude faster than Flex ddG, taking less than 0.1 seconds per mutation using a H100 GPU. It took 10 and 5 hours respectively to fine-tune STAB-DDG on the Megascale dataset and the SKEMPIv2.0 training split on a single H100 GPU. Flex ddG took 15 CPU hours per mutation with 10 models and 35,000 backrub steps.

**Stratification of performance.** To understand how STAB-DDG performs on different types of complexes, we performed an analysis on different subsets of the binding data test set. We stratified the test set according to interface rigidity and complex size (Table 3). As a proxy for interface rigidity, we computed the loop content at the interface; specifically, we considered all residues within 10 Å of an atom in another chain and computed the fraction of these residues with secondary structure annotated as loop. We found that STAB-DDG performed better for more rigid, smaller complexes.

The better performance on rigid interfaces may be explained by STAB-DDG’s use of a single static structure for prediction of folding energy for both the complex and monomers; flexible interfaces are more likely to change upon binding and will be less well represented by a single structure.

The better performance on smaller complexes may be explained by the bias in the composition of the folding stability data of Tsuboyama et al. (2023), which consists only of small <80 residue domains.

Table 3. Performance of STAB-DDG across stratification of binding test set; Root Mean Squared Error (RMSE) in Kcal/mol for different interface loop content and complex size (number of residues) thresholds.

Loop Content	RMSE	Complex Size	RMSE
< 30%	1.12	< 150	0.94
< 40%	1.29	< 200	0.99
< 50%	1.46	< 400	1.28
< 60%	1.50	< 600	1.42
< 70%	1.48	< 800	1.38
< 80%	1.48	< 1000	1.50

### 5.3. Generalization of prediction performance on two case study datasets.

Despite STAB-DDG having achieved state-of-the-art performance on SKEMPIv2.0, the statistical power of the con-

<sup>1</sup><https://github.com/LDeng0205/binding-ddg>.

clusions drawn were limited by the size of the dataset and experimental noise. Thus, it remains to be validated whether our conclusions still hold and if current computational binding  $\Delta\Delta G$  prediction tools are readily useful in settings not represented in SKEMPIv2.0. We sought to address this problem by evaluating STAB-DDG in two case studies, de novo designed “mini-binder” yeast surface display binding dataset and a curated TCR mimic dataset.

**Yeast surface display case study.** To validate the effects of fine-tuning on folding stability data and further fine-tuning on binding data, we compared STAB-DDG zero-shot, Stability fine-tuned, and STAB-DDG on site saturation mutagenesis data from Cao et al. (2022), which has been used to perform retrospective evaluation of DL-based binder design methods (Bennett et al., 2023; Zambaldi et al., 2024). The dataset contains sequence count information from yeast surface display libraries of 28,293 single mutants across 33 complexes. The sequence counts are then used to estimate a proxy for the dissociation constants for each binder which we then relate to a  $\Delta\Delta G$  estimate (Appendix E).

We found that both fine-tuning on folding stability and binding affinity improved binding prediction accuracy (Figure 4). However, we found that the folding energy predictor for the entire complex achieved a higher per interface Spearman than our binding predictor parameterization. Appendix E demonstrates this observation is explained through the experimental readout confounding expression levels with binding energy in the yeast-display based assay. In brief, the binding energy proxy of a particular variant depends both on its binding affinity and its expression, a quantity closely related to folding stability.

**TCRm case study.** We curated a set of 30  $\Delta\Delta G$  measurements from six TCR mimic structures determined by surface plasmon resonance (SPR) by searching through all TCR mimic structures in the TCR3d database (Appendix A) (Gowthaman & Pierce, 2019). To assess the utility of STAB-DDG in the TCR mimic design task for cancer therapy, we next evaluated STAB-DDG and Flex ddG on these data (Table 4). We found that STAB-DDG is not conclusively useful based on the limited TCRm case study set.

Table 4. Evaluation of  $\Delta\Delta G$  prediction on the TCR mimic case study dataset. Area Under the Receiver Characteristic (AUROC) is computed on the binary classification task of whether a mutation increases binding affinity ( $\Delta\Delta G < 0$ ). Standard errors are obtained from cluster-bootstrapping (see Appendix C).

	SPEARMAN	RMSE	AUROC
FLEX DDG	$0.15 \pm 0.27$	$1.44 \pm 0.30$	$0.49 \pm 0.21$
STAB-DDG	$0.13 \pm 0.39$	$1.26 \pm 0.24$	$0.58 \pm 0.25$



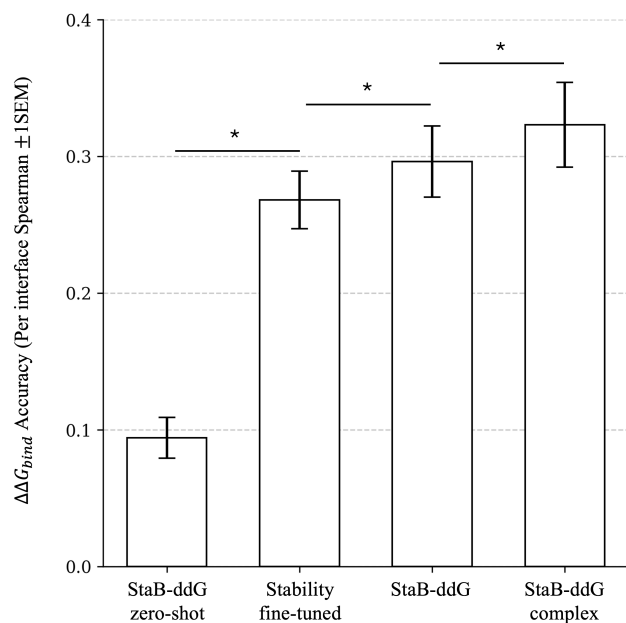


Figure 4. Comparison of STAB-DDG zero-shot, Stability fine-tuned model, and STAB-DDG on the yeast surface display dataset. \* denotes significance (one-sided paired t-test) at  $p < 0.05$ .

## 6. Discussion

Accurate computational prediction of the mutational effects on protein interaction binding energies could significantly improve the potency and specificity of protein therapeutics. Despite years of interest in improving such predictions with deep learning, success has been minimal. By achieving performance comparable to Flex ddG, StaB-ddG marks an important step in this direction.

Computational prediction of mutational effects on binding energies remains a challenging open problem. Several areas remain to be explored. First, STAB-DDG does not model changes in the backbone upon a mutation; in general, mutations on flexible regions of the binding site are likely to introduce fluctuations in the backbone structure. A future method incorporating such structural changes could improve binding energy estimators like STAB-DDG. Furthermore, the extent to which the scarcity of available binding data and therefore, scaling laws, impacts the accuracy of current models necessitates further investigation.

## Acknowledgements

We would like to thank Sebastian Thrun for providing useful guidance on the research direction. We would like to thank Henry Dieckhaus, Brian Kuhlman, and Gabriel Rocklin for helpful discussions. We would also like to thank Sebastian Thrun, Christopher Fifty, James Bowden, Henry Smith, and Nate Diamant for help reviewing the manuscript.

## Impact Statement

This paper presents work whose goal is to advance the machine learning methods for modeling and design of proteins. There are many potential societal consequences of our work, none which we feel must be specifically highlighted.

## References

- Abramson, J., Adler, J., Dunger, J., Evans, R., Green, T., Pritzel, A., Ronneberger, O., Willmore, L., Ballard, A. J., Bambrick, J., et al. Accurate structure prediction of biomolecular interactions with AlphaFold 3. *Nature*, 2024.
- Barlow, K. A., O Conchuir, S., Thompson, S., Suresh, P., Lucas, J. E., Heinonen, M., and Kortemme, T. Flex ddG: Rosetta ensemble-based estimation of changes in protein-protein binding affinity upon mutation. *The Journal of Physical Chemistry B*, 2018.
- Bennett, N. R., Coventry, B., Goreshnik, I., Huang, B., Allen, A., Vafeados, D., Peng, Y. P., Dauparas, J., Baek, M., Stewart, L., et al. Improving de novo protein binder design with deep learning. *Nature Communications*, 2023.
- Birnbaum, M. E., Mendoza, J. L., Sethi, D. K., Dong, S., Glanville, J., Dobbins, J., Özkan, E., Davis, M. M., Wucherpennig, K. W., and Garcia, K. C. Deconstructing the peptide-MHC specificity of T cell recognition. *Cell*, 2014.
- Bushuiev, A., Bushuiev, R., Kouba, P., Filkin, A., Gabrielova, M., Gabriel, M., Sedlar, J., Pluskal, T., Damborsky, J., Mazurenko, S., and Sivic, J. Learning to design protein-protein interactions with enhanced generalization. In *International Conference on Learning Representations*, 2024.
- Cameron, A. C. and Miller, D. L. A practitioner’s guide to cluster-robust inference. *Journal of human resources*, 2015.
- Cao, L., Coventry, B., Goreshnik, I., Huang, B., Sheffler, W., Park, J. S., Jude, K. M., Marković, I., Kadam, R. U., Verschueren, K. H., et al. Design of protein-binding proteins from the target structure alone. *Nature*, 2022.
- Dauparas, J., Anishchenko, I., Bennett, N., Bai, H., Ragotte, R. J., Milles, L. F., Wicky, B. I., Courbet, A., de Haas, R. J., Bethel, N., et al. Robust deep learning-based protein sequence design using ProteinMPNN. *Science*, 2022.
- Diaz, D. J., Gong, C., Ouyang-Zhang, J., Loy, J. M., Wells, J., Yang, D., Ellington, A. D., Dimakis, A. G., and Klivans, A. R. Stability Oracle: a structure-based graph-

- transformer framework for identifying stabilizing mutations. *Nature Communications*, 2024.
- Dieckhaus, H., Brocidiacono, M., Randolph, N. Z., and Kuhlman, B. Transfer learning to leverage larger datasets for improved prediction of protein stability changes. *Proceedings of the National Academy of Sciences*, 2024.
- Dourado, D. F. and Flores, S. C. A multiscale approach to predicting affinity changes in protein-protein interfaces. *Proteins: Structure, Function, and Bioinformatics*, 2014.
- Gowthaman, R. and Pierce, B. G. TCR3d: The T cell receptor structural repertoire database. *Bioinformatics*, 2019.
- Hammersley, J. M. and Morton, K. W. A new Monte Carlo technique: antithetic variates. In *Mathematical proceedings of the Cambridge philosophical society*. Cambridge University Press, 1956.
- Hastie, T., Tibshirani, R., and Friedman, J. H. The elements of statistical learning: data mining, inference, and prediction, 2009.
- Holland, C. J., Crean, R. M., Pentier, J. M., de Wet, B., Lloyd, A., Srikannathasan, V., Lissin, N., Lloyd, K. A., Blicher, T. H., Conroy, P. J., et al. Specificity of bispecific T cell receptors and antibodies targeting peptide-HLA. *The Journal of clinical investigation*, 2020.
- Hopf, T. A., Ingraham, J. B., Poelwijk, F. J., Schärfe, C. P., Springer, M., Sander, C., and Marks, D. S. Mutation effects predicted from sequence co-variation. *Nature biotechnology*, 2017.
- Householder, K. D., Xiang, X., Jude, K. M., Deng, A., Obenaus, M., Wilson, S. C., Chen, X., Wang, N., and Garcia, K. C. De novo design and structure of a peptide-centric TCR mimic binding module. *bioRxiv*, 2024.
- Hsiue, E. H.-C., Wright, K. M., Douglass, J., Hwang, M. S., Mog, B. J., Pearlman, A. H., Paul, S., DiNapoli, S. R., König, M. F., Wang, Q., et al. Targeting a neoantigen derived from a common TP53 mutation. *Science*, 2021.
- Hsu, C., Nisonoff, H., Fannjiang, C., and Listgarten, J. Learning protein fitness models from evolutionary and assay-labeled data. *Nature biotechnology*, 2022a.
- Hsu, C., Verkuil, R., Liu, J., Lin, Z., Hie, B., Sercu, T., Lerer, A., and Rives, A. Learning inverse folding from millions of predicted structures. In *International Conference on Machine Learning*. PMLR, 2022b.
- Hwang, M. S., Miller, M. S., Thirawatananond, P., Douglass, J., Wright, K. M., Hsiue, E. H.-C., Mog, B. J., Aytenfisu, T. Y., Murphy, M. B., Aitana Azurmendi, P., et al. Structural engineering of chimeric antigen receptors targeting HLA-restricted neoantigens. *Nature communications*, 2021.
- Jankauskaitė, J., Jiménez-García, B., Dapkūnas, J., Fernández-Recio, J., and Moal, I. H. SKEMPI 2.0: an updated benchmark of changes in protein-protein binding energy, kinetics and thermodynamics upon mutation. *Bioinformatics*, 2019.
- Jiao, X., Mao, W., Jin, W., Yang, P., Chen, H., and Shen, C. Boltzmann-Aligned inverse folding model as a predictor of mutational effects on protein-protein interactions. *arXiv preprint arXiv:2410.09543*, 2024.
- Johansen, K. H., Wolff, D., Scapolo, B., Fernandez-Quintero, M. L., Christensen, C. R., Loeffler, J. R., Rivera-de Torre, E., Overath, M. D., Munk, K. K., Morell, O., et al. De novo designed pMHC binders facilitate T cell induced killing of cancer cells. *bioRxiv*, 2024.
- Kastritis, P. L. and Bonvin, A. M. On the binding affinity of macromolecular interactions: daring to ask why proteins interact. *Journal of The Royal Society Interface*, 2013.
- Klebanoff, C. A., Chandran, S. S., Baker, B. M., Quezada, S. A., and Ribas, A. T cell receptor therapeutics: immunological targeting of the intracellular cancer proteome. *Nature Reviews Drug Discovery*, 2023.
- Kumar, A., Raghunathan, A., Jones, R., Ma, T., and Liang, P. Fine-tuning can distort pretrained features and underperform out-of-distribution. *arXiv preprint arXiv:2202.10054*, 2022.
- Lapedes, A., Giraud, B., and Jarzynski, C. Using sequence alignments to predict protein structure and stability with high accuracy. *arXiv preprint arXiv:1207.2484*, 2012.
- Li, D., Brackenridge, S., Walters, L. C., Swanson, O., Harlos, K., Rozbesky, D., Cain, D. W., Wiehe, K., Searce, R. M., Barr, M., et al. Mouse and human antibodies bind HLA-E-leader peptide complexes and enhance NK cell cytotoxicity. *Communications Biology*, 2022.
- Linette, G. P., Stadtmauer, E. A., Maus, M. V., Rapoport, A. P., Levine, B. L., Emery, L., Litzky, L., Bagg, A., Carreno, B. M., Cimino, P. J., et al. Cardiovascular toxicity and titin cross-reactivity of affinity-enhanced T cells in myeloma and melanoma. *Blood, The Journal of the American Society of Hematology*, 2013.
- Liu, B., Greenwood, N. F., Bonzanini, J. E., Motmaen, A., Sharp, J., Wang, C., Visani, G. M., Vafeados, D. K., Roullier, N., Nourmohammad, A., et al. Design of high specificity binders for peptide-MHC-I complexes. *bioRxiv*, 2024a.

- Liu, S., Zhu, T., Ren, M., Yu, C., Bu, D., and Zhang, H. Predicting mutational effects on protein-protein binding via a side-chain diffusion probabilistic model. *Advances in Neural Information Processing Systems*, 2024b.
- Luo, S., Su, Y., Wu, Z., Su, C., Peng, J., and Ma, J. Rotamer density estimator is an unsupervised learner of the effect of mutations on protein-protein interaction. In *International Conference on Learning Representations*, 2023.
- Mo, Y., Hong, X., Gao, B., Jia, Y., and Lan, Y. Multi-level interaction modeling for protein mutational effect prediction. *arXiv preprint arXiv:2405.17802*, 2024.
- Notin, P., Kollasch, A., Ritter, D., Van Niekerk, L., Paul, S., Spinner, H., Rollins, N., Shaw, A., Orenbuch, R., Weitzman, R., et al. Proteingym: Large-scale benchmarks for protein fitness prediction and design. *Advances in Neural Information Processing Systems*, 2023.
- Park, H., Bradley, P., Greisen Jr, P., Liu, Y., Mulligan, V. K., Kim, D. E., Baker, D., and DiMaio, F. Simultaneous optimization of biomolecular energy functions on features from small molecules and macromolecules. *Journal of chemical theory and computation*, 2016.
- Riesselman, A. J., Ingraham, J. B., and Marks, D. S. Deep generative models of genetic variation capture the effects of mutations. *Nature methods*, 2018.
- Rives, A., Meier, J., Sercu, T., Goyal, S., Lin, Z., Liu, J., Guo, D., Ott, M., Zitnick, C. L., Ma, J., et al. Biological structure and function emerge from scaling unsupervised learning to 250 million protein sequences. *Proceedings of the National Academy of Sciences*, 2021.
- Rossjohn, J., Gras, S., Miles, J. J., Turner, S. J., Godfrey, D. I., and McCluskey, J. T cell antigen receptor recognition of antigen-presenting molecules. *Annual review of immunology*, 2015.
- Sampson, J. M., Cannon, D. A., Duan, J., Epstein, J. C., Sergeeva, A. P., Katsamba, P. S., Mannepalli, S. M., Bahna, F. A., Adihou, H., Gu  ret, S. M., et al. Robust prediction of relative binding energies for protein-protein complex mutations using free energy perturbation calculations. *Journal of Molecular Biology*, 2024.
- Schymkowitz, J., Borg, J., Stricher, F., Nys, R., Rousseau, F., and Serrano, L. The FoldX web server: an online force field. *Nucleic acids research*, 2005.
- Sergeeva, A. P., Katsamba, P. S., Liao, J., Sampson, J. M., Bahna, F., Mannepalli, S., Morano, N. C., Shapiro, L., Friesner, R. A., and Honig, B. Free energy perturbation calculations of mutation effects on SARS-CoV-2 RBD::ACE2 binding affinity. *Journal of Molecular Biology*, 2023.
- Stewart-Jones, G., Wadle, A., Hombach, A., Shenderov, E., Held, G., Fischer, E., Kleber, S., Nuber, N., Stenner-Liewen, F., Bauer, S., et al. Rational development of high-affinity T-cell receptor-like antibodies. *Proceedings of the National Academy of Sciences of the United States of America*, 2009.
- Sun, Y., Florio, T. J., Gupta, S., Young, M. C., Marshall, Q. F., Garfinkle, S. E., Papadaki, G. F., Truong, H. V., Mycek, E., Li, P., et al. Structural principles of peptide-centric chimeric antigen receptor recognition guide therapeutic expansion. *Science immunology*, 2023.
- Tsuboyama, K., Dauparas, J., Chen, J., Laine, E., Mohseni Behbahani, Y., Weinstein, J. J., Mangan, N. M., Ovchinnikov, S., and Rocklin, G. J. Mega-scale experimental analysis of protein folding stability in biology and design. *Nature*, 2023.
- Watson, J. L., Juergens, D., Bennett, N. R., Trippe, B. L., Yim, J., Eisenach, H. E., Ahern, W., Borst, A. J., Ragotte, R. J., Milles, L. F., et al. De novo design of protein structure and function with RFdiffusion. *Nature*, 2023.
- Wright, K. M., DiNapoli, S. R., Miller, M. S., Aitana Azurmendi, P., Zhao, X., Yu, Z., Chakrabarti, M., Shi, W., Douglass, J., Hwang, M. S., et al. Hydrophobic interactions dominate the recognition of a KRAS G12V neoantigen. *Nature communications*, 2023.
- Wu, F. and Li, S. Z. Surface-vqmae: Vector-quantized masked auto-encoders on molecular surfaces. In *International Conference on Machine Learning*, 2024.
- Wu, L., Tian, Y., Lin, H., Huang, Y., Li, S., Chawla, N. V., and Li, S. Z. Learning to predict mutation effects of protein-protein interactions by microenvironment-aware hierarchical prompt learning. *arXiv preprint arXiv:2405.10348*, 2024.
- Yang, X., Nishimiya, D., L  chte, S., Jude, K. M., Borowska, M., Savvides, C. S., Dougan, M., Su, L., Zhao, X., Piehler, J., et al. Facile repurposing of peptide-MHC-restricted antibodies for cancer immunotherapy. *Nature Biotechnology*, 2023.
- Zambaldi, V., La, D., Chu, A. E., Patani, H., Danson, A. E., Kwan, T. O., Frerix, T., Schneider, R. G., Saxton, D., Thillaisundaram, A., et al. De novo design of high-affinity protein binders with AlphaProteo. *arXiv preprint arXiv:2409.08022*, 2024.
- Zwanzig, R. W. High-temperature equation of state by a perturbation method. I. Nonpolar gases. *The Journal of Chemical Physics*, 1954.

## Appendix Table of Contents

---

<b>A.</b>	Additional background on binding $\Delta\Delta G$ prediction and TCR mimic engineering
<b>B.</b>	Thermodynamic properties
<b>C.</b>	SKEMPIv2.0 filtering and metrics
<b>D.</b>	Additional experiments on variations of STAB-DDG
<b>E.</b>	Additional details on the main text results

---



## A. Additional background on binding $\Delta\Delta G$ prediction and TCR mimic engineering

### A.1. Background

**Binding specificity.** The binding specificity of a protein can be characterized by the difference in binding affinity between the reference, or wild-type, interaction and off-target interactions, where binding affinity is the free energy difference ( $\Delta G$ ) between the bound and unbound states of a system of two proteins. More concretely, a binding affinity difference of  $\Delta\Delta G = 1 \text{ kcal/mol}$  between a cancer target and its healthy analogue would translate to 10X higher binding affinity for the cancer target. Thus, binding specificity can be expressed by a series of  $\Delta\Delta G$  values between the wild type interaction and a known list of off-targets.

**TCR mimic specificity.** TCR mimic antibodies hold significant promise for cancer-specific immunotherapy (Klebanoff et al., 2023; Yang et al., 2023). These engineered molecules are designed to selectively bind to cancer-associated peptides presented on major histocompatibility complexes (pMHCs) while avoiding recognition of off-target peptides displayed on healthy cells. Given that these peptides are typically only 9–12 amino acids long, the challenge lies in distinguishing cancer-associated pMHCs from normal pMHCs, which can sometimes differ by just a single amino acid (Rossjohn et al., 2015). Achieving this level of specificity is critical, as even minor cross-reactivity could lead to severe dose-limiting toxicities or fatal depletion of essential healthy cells (Linette et al., 2013). Predicting off-target toxicity is particularly difficult because the potential peptide landscape is vast—ranging from approximately  $20^9$  to  $20^{12}$  theoretical peptide combinations. As a result, experimental screening alone is often insufficient to fully assess specificity (Birnbbaum et al., 2014; Holland et al., 2020). Computational approaches that refine TCR mimic binding to maximize selectivity could significantly reduce toxicity risks while enhancing precision and the molecule’s therapeutic window. By improving specificity, such strategies could accelerate the development of safer and more effective TCR mimic therapies, ultimately broadening their clinical utility.

### A.2. TCR mimic case study

To curate this case study, we searched the TCR3d Database for structures of TCR mimic antibodies bound to pMHC that were deposited in the PDB and had associated surface plasmon resonance (SPR) data with mutations (Gowthaman & Pierce, 2019). We prioritized SPR data because it provides the most quantitatively accurate and sensitive measurements of binding affinity changes, making it a reliable source of binding  $\Delta\Delta G$ . TCR mimic antibodies contain flexible loops with many degrees of freedom, making the effects of mutations on affinity and specificity particularly difficult to predict. In total, we identified six TCR mimic complexes with available mutational and SPR data from the literature (PDB IDs: 3HAE, 6UJ9, 6W51, 7BH8, 7STF, 8EK5) (Stewart-Jones et al., 2009; Hwang et al., 2021; Hsiue et al., 2021; Li et al., 2022; Wright et al., 2023; Sun et al., 2023). These complexes exhibited a diversity of mutation sites, including mutations on the TCR mimic loops, the peptide, and the MHC, as well as a mix of single and multiple mutations. For each structure, we calculated the ground truth  $\Delta\Delta G$  based on changes in binding affinity from the wild-type to the mutant protein. In cases where a mutation resulted in undetectable affinity by SPR, we estimated the mutant protein’s affinity to be 100,000 nM—a conservative approximation given that true affinity values in such cases are often much weaker. This threshold effectively reflects a significant loss of binding, as interactions with affinities above 100,000 nM are generally considered too weak for physiological relevance (Table 5). Finally, we compared these experimental  $\Delta\Delta G$  values to the predicted  $\Delta\Delta G$  values generated by  $\Delta\Delta G$ , allowing us to assess the predictive accuracy of computational models for binding energy changes in TCR mimic systems.

Table 5. TCR mimic case study dataset.

Pdb	Mutation(s)	$\Delta\Delta G$ (kcal/mol)	Notes
8ek5	EA59A	0.428314	HLA mutation; Figure 1J
8ek5	EA63A	No binding	HLA mutation; Figure 1J
8ek5	QA73A	2.427024	HLA mutation; Figure 1J
8ek5	TA74A	1.037010	HLA mutation; Figure 1J
8ek5	QA156A	-0.185302	HLA mutation; Figure 1J
8ek5	TA164A	0.020049	HLA mutation; Figure 1J
8ek5	QC1A	0.151418	peptide mutation; Supp. Figure S16
8ek5	NC3A	1.900784	peptide mutation; Supp. Figure S16
8ek5	PC4A	0.218890	peptide mutation; Supp. Figure S16
8ek5	IC5A	1.853897	peptide mutation; Supp. Figure S16
8ek5	RC6A	No binding	peptide mutation; Supp. Figure S16
8ek5	TC7A	1.571367	peptide mutation; Supp. Figure S16
8ek5	TC8A	0.716476	peptide mutation; Supp. Figure S16
8ek5	IC5L	0.433947	peptide mutation; estimated Kd values
8ek5	IC5V	0.921828	peptide mutation; estimated Kd values
8ek5	IC5G	2.163521	peptide mutation; estimated Kd values
7stf	VC12G	No binding	peptide mutation
7stf	FL53W	-0.299732	TCRm mutation
7stf	VH104N	0.436337	TCRm mutation
7stf	VH104R	-0.421575	TCRm mutation
7stf	VH104R,VC12G	1.431891	TCRm and peptide mutation
7bh8	YG97S,YG98A,GG99Q,SG100Y	-1.394408	TCRm mutations (affinity maturation)
7bh8	YG97G,YG98A,GG99Q,SG100W	-1.132139	TCRm mutations (affinity maturation)
6uj9	QC7R	0.760277	peptide mutation; residue faces inside HLA groove
6uj9	YH103H,QC7R	No binding	TCRm and peptide mutation
6uj9	YH103H	0.355047	TCRm mutation
6w51	HF8R	No binding	peptide mutation
3hae	SL26E,SL96G	-0.628096	T1 mutant vs. 3M4E5 TCR mimic
3hae	SL26E,SL96G,VC9C	-0.806352	T1 mutant with peptide anchor residue mutation
3hae	VC9C	0.005531	peptide anchor residue mutation only

## B. Theoretical properties of a StaB-ddG and $\Delta\Delta G_{\text{bind}}$ predictors

In this section, we first provide a complete statement of Expressivity in Proposition 3.1. We then discuss all three properties for each of the other predictors in Table 1. Our statement of relies on a dataset of binding  $\Delta\Delta G$  measurements of the form introduced in Section 3.2.

**Proposition B.1** (Proposition 3.1, Expressivity (formal)). *For any  $\mathcal{D}$ , there exists  $\Delta b_\theta \in \mathcal{B}$  such that*

$$\Delta b_\theta(s_{n,\text{ref}}, s_{n,m}) = y_{n,m}$$

for all  $(x_n, s_{n,\text{ref}}, s_{n,m}, y_{n,m}) \in \mathcal{D}$ .

### B.1. Proof of Proposition 3.1

**Expressivity.** Consider a simplex-valued function that for each  $n = 1, \dots, N$  satisfies  $p_\theta(s_{n,\text{ref}}|x_n) \propto \exp\{y_{n,\text{ref}}\}$  and for each  $m = 1, \dots, M_n$ ,  $p_\theta(s_{n,m}|x_n) \propto \exp\{y_{n,m}\}$ . Notice that  $\log p_\theta(s_{n,\text{ref}}|x) = y_{n,\text{ref}} + c$  and  $\log p_\theta(s_{n,m}|x) = y_{n,m} + c$  where  $c$  is a constant. The corresponding function  $\Delta b_\theta \in \mathcal{B}$  therefore satisfies  $\Delta b_\theta(s_{n,\text{ref}}, s_{n,m}|x_n) = \log p_\theta(s_{n,\text{ref}}|x) - \log p_\theta(s_{n,m}|x) = y_{n,m} - y_{n,\text{ref}}$ .

### B.2. Thermodynamic properties of other predictors

**Flex ddG.** The Flex ddG predictor uses the same thermodynamic identity in Equation 1 and Equation 2 to parametrize binding  $\Delta\Delta G$ , and uses the Rosetta energy function to predict the folding  $\Delta G$  terms. As such, the Flex ddG predictor satisfies Antisymmetry and Mutational path independence. However, the Expressivity of the predictor is fundamentally limited by the parametric form of the empirical energy function, which cannot provide close approximations to arbitrary functions.

**RDE-Net.** RDE-Net first creates neural network embeddings  $h_{wt}$  and  $h_{mut}$  for the wildtype and mutant respectively. The embeddings are then used as input to another neural network, denoted by MLP. The final output is computed as  $(\text{MLP}(h_{mut} - h_{wt}) - \text{MLP}(h_{wt} - h_{mut}))/2$ , which enforces Antisymmetry by construction. However, since MLP is in general not a linear function, there is no guarantee on Mutational path independence. Lastly, using the same proof as above, it can be shown that the neural network parametrization satisfies Expressivity.

**PPIformer.** PPIformer uses a masked language model to model sequence likelihood. The final predictor looks similar to  $\Delta f_\theta$ :

$$\widehat{\Delta\Delta G} = \sum_{i \in M} \log p(\hat{c}_i = s_i | s_{\setminus M}) - \sum_{i \in M} \log p(\hat{c}_i = m_i | s_{\setminus M}).$$

In the above,  $M$  is a set of mutated positions, where  $s_i$  denotes the wildtype amino acid and  $m_i$  denotes the mutant amino acid for position  $i$ . The PPIformer predictor also satisfies Antisymmetry by construction. However, it does not satisfy Mutational path independence as the conditioning information,  $c_{\setminus M}$ , depends on the difference between wildtype and the mutant. As such, the conditioning information between two pairs of sequences will be different. Lastly, each mutated position is predicted independently from the other mutated positions. As such, the predictor enforces the effects between any set of mutations to be additive. The enforced additivity does not satisfy Expressivity as mutations generally involve non-additive effects.

**Other predictors.** Surface-VQMAE, Prompt-DDG, DiffAffinity and ProMIM are parametrized by multilayer perceptrons that take as input embeddings from another neural network, without any guarantees of Antisymmetry or Mutational path independence. However, these predictors are expressive, treating neural networks as expressive functions.

## C. SKEMPIv2.0 filtering and metrics

In this section we outline the dataset filtering and splitting details and discuss the “per interface” metrics.

### C.1. SKEMPIv2.0 filtering and splitting procedure

The original SKEMPIv2 dataset contains 7,085 mutant entries. We filter and split SKEMPIv2.0 according to the following steps.

1. Remove 285 mutants with missing affinity measurements.
2. Remove 884 duplicate mutants with the same mutations on the same crystal structure.
3. Remove 1,029 mutants that only contain mutations at non-interface residues. We remove these because mutations at non-interface residues do not have significant contributions to binding affinity changes (Dourado & Flores, 2014).
4. Remove 108 complexes with less than 3 mutants assayed. This reduces the bias and noise from different experimental conditions.
5. Remove 4 complexes with more than 40% of the measured  $\Delta\Delta G$  to be the same value. This removes 49 mutants.
6. Remove 8 complexes with unresolved residues in the crystal structure. This removes 162 mutants.

After these filtering steps, we have 201 complexes and 4,541 mutants. We cluster the complexes using the original SKEMPIv2.0 clusters based on structural homology near the binding site, resulting in 64 disjoint clusters (Jankauskaitė et al., 2019). Then, we perform a random splitting to obtain 20 clusters with 1,491 mutants across 81 complexes as our test set. We report these clusters and split at <https://github.com/LDeng0205/binding-ddG>.

### C.2. Additional metrics for evaluating binding prediction accuracy

We introduce additional metrics for assessing prediction accuracy: Pearson correlation, Root Mean Squared Error (RMSE), and Area Under the Receiver Characteristic (AUROC). AUROC is computed on the binary classification task of whether a mutation increases binding affinity ( $\Delta\Delta G < 0$ ). We additionally compute the “overall” metrics for the entire set of predictions that include different complexes. For each overall metric, we can compute a standard error as the standard deviation of that metric on cluster-bootstrap resample of the test set where on each bootstrap sample we draw full complexes from the test set complexes with replacement (Cameron & Miller, 2015). These standard errors approximate the variability in the overall metrics owing to the choice of structures included in the test set.

The “per interface” metrics reported in Table 8 are obtained by computing each metric for each complex, then take the average across complexes. For complexes that contain less than 10 mutants, the correlation values obtained are empirically observed to be noisy (Figure 5). As such, we decide to report the mean of metrics for complexes with 10 or more mutants to reduce the effect of noise. We examine the impact of the choice of such a threshold on the relative performance between STAB-DDG andm Flex ddG (Figure 6). We find that the relative performance is robust to the choice of the threshold.



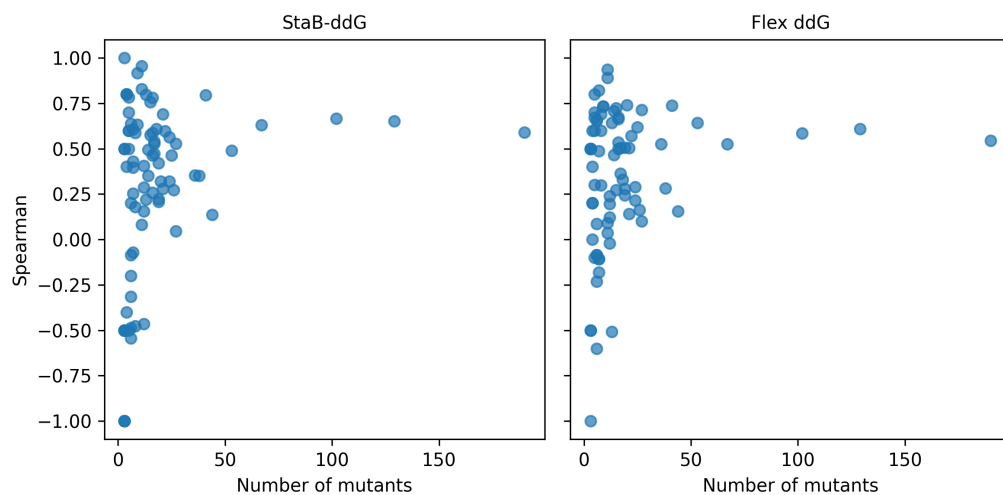


Figure 5. Spearman correlation vs. Number of mutants. Each point represents a complex.

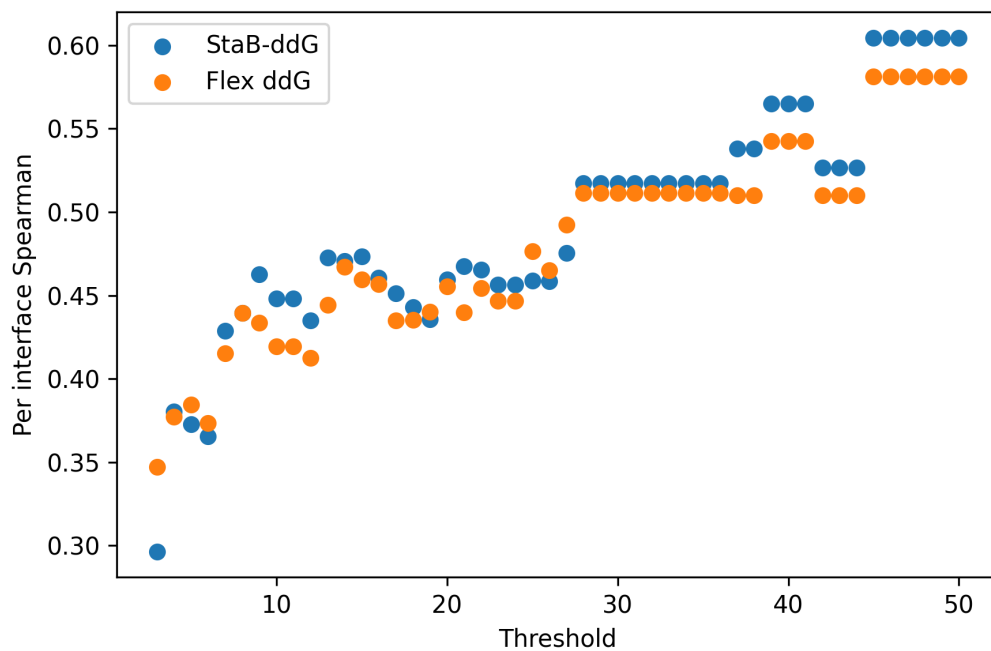


Figure 6. The relative performance of models for different thresholds when computing per interface spearman.

## D. Additional experiments on variations of STAB-DDG

### D.1. Linear model initialization

Tsuboyama et al. (2023) proposed to use amino acid-specific offsets in a model relating sequence probabilities in protein families to stability measurements. We experimented with a similar approach and introduce a linear model on top of our folding  $\Delta\Delta G$  predictor as

$$F(s, s') = \alpha \Delta f_\theta(s, s') + \left( \sum_{a \in s} \phi_a - \sum_{a \in s'} \phi_a \right) + \phi_0 \quad (9)$$

where  $\alpha$  is a scaling term to correct for the initial scale mismatch,  $\phi_0$  is a global bias, and  $\phi_a$  represents amino-acid specific offsets. We fit the linear parameters first with the zero-shot predictor  $\Delta f_\theta(s, s')$  before fine-tuning  $\theta$ . This procedure is inspired by the idea that fine-tuning the last layers of a neural network first could help improve generalization performance (Kumar et al., 2022). We use a predictor of the following form

$$B(s, s') = \alpha \Delta b_\theta(s, s') + \left( \sum_{a \in s} \phi_a - \sum_{a \in s'} \phi_a \right) + \phi_0 \quad (10)$$

which uses the same set of linear weights as  $F$ . Note that the linear model introduces asymmetry and the updated predictors no longer satisfy the first two properties of Proposition 3.1.

We found that fitting the linear model and following the same fine-tuning procedure, with  $F$  and  $B$  as folding and binding predictors, did not lead to a significant difference in prediction accuracy (Table 7).

We provide the fitted linear parameters  $\alpha$ ,  $\phi_0$ , and  $\phi_a$  in Table 6. The learned  $\phi_0$  is negative, indicating that most mutations in the dataset are destabilizing. In addition, the offset for TRP, a bulky hydrophobic residue expected to have larger effects on stability, is the second largest in magnitude and is negative (destabilizing).

Table 6. Linear parameter values.

$\alpha$	$\phi_0$	ALA	CYS	ASP	GLU	PHE	GLY	HIS	ILE	LYS	LEU	MET
0.24	-0.19	0.00	-0.80	0.04	0.10	-0.55	0.13	-0.20	-0.40	0.12	-0.33	-0.47

ASN	PRO	GLN	ARG	SER	THR	VAL	TRP	TYR
0.01	0.33	-0.01	-0.23	0.00	-0.07	-0.27	-0.68	-0.50

### D.2. Using AlphaFold 3 predictions for apo structures

We experimented with using AlphaFold 3 (Abramson et al., 2024) predicted structures for individual binders instead of obtaining them from the complex crystal structure. We hypothesized that this would more closely track the apo (unbound) state of the structures for more accurate folding energy predictions. We found this to have not made a significant difference in the Per interface Spearman metric, but have improved several other metrics (Table 7).

### D.3. Normalizing complex loss with the number of mutants

In our fine-tuning objective (Equation (8)), we weight each complex  $n$  by the number of mutants assayed  $M_n$ . We additionally experimented with weighting the loss by  $\sqrt{M_n}$  instead of  $M_n$ . However, we did not find a significant difference between the two weighting schemes (Table 7).

### D.4. Variance reduction

We evaluated the effects of antithetic variates and the number of Monte Carlo samples on reducing prediction error, measured by RMSE (Figure 7). We found that the antithetic variates method significantly reduced prediction error, and Monte Carlo ensembling further reduced the error. In addition to improving prediction accuracy at inference time, fixing the decoding order and backbone noise also led to better training dynamics. In particular, under the same hyperparameters, a model trained without fixing these additional parameters performed much worse than STAB-DDG (Table 7). In our other experiments, we ensemble over 20 samples.

### D.5. Ablations

**Fine-tuning on folding stability data without inverse-folding pre-training.** We randomly initialized weights to our predictor and fine-tuned it on folding stability data. We found that the performance was much worse than STAB-DDG zero-shot, suggesting that pre-training contributes significantly to model performance (Table 7).

**Fine-tuning on binding affinity data from ProteinMPNN weights.** We directly fine-tuned STAB-DDG zero-shot on binding energy data without incorporating folding stability data. We found that though the per interface metrics remained the same, the overall accuracy dropped (Table 7).

Table 7. Evaluation of prediction performance of variations of STAB-DDG on the test split of SKEMPIv2.0. Per interface metrics for which the difference from STAB-DDG is not statistically significant are underlined. Statistical significance is determined by a paired, one-sided t-test against STAB-DDG. Standard errors are also reported for per interface metrics.

Method	Per Interface			Overall			
	Pearson	Spearman	RMSE	Pearson	Spearman	RMSE	AUROC
StaB-ddG	$0.49 \pm 0.04$	$0.45 \pm 0.04$	$1.41 \pm 0.12$	$0.53 \pm 0.06$	$0.53 \pm 0.06$	$1.72 \pm 0.11$	$0.73 \pm 0.05$
No folding	$0.50 \pm 0.04$	$0.46 \pm 0.04$	<u><math>1.53 \pm 0.13</math></u>	$0.47 \pm 0.07$	$0.47 \pm 0.05$	$1.92 \pm 0.13$	$0.70 \pm 0.04$
No pre-train	$0.12 \pm 0.05$	$0.12 \pm 0.05$	$2.04 \pm 0.15$	$0.23 \pm 0.07$	$0.17 \pm 0.05$	$2.41 \pm 0.14$	$0.61 \pm 0.04$
No ant. var.	$0.30 \pm 0.04$	$0.30 \pm 0.04$	$1.96 \pm 0.16$	$0.19 \pm 0.08$	$0.17 \pm 0.06$	$2.35 \pm 0.17$	$0.58 \pm 0.05$
Linear model	$0.47 \pm 0.04$	$0.44 \pm 0.04$	<u><math>1.52 \pm 0.14</math></u>	$0.54 \pm 0.05$	$0.49 \pm 0.05$	$1.79 \pm 0.11$	$0.72 \pm 0.04$
Pred. apo structures	<u><math>0.45 \pm 0.05</math></u>	<u><math>0.43 \pm 0.04</math></u>	<u><math>1.43 \pm 0.10</math></u>	$0.60 \pm 0.05$	$0.56 \pm 0.05$	$1.66 \pm 0.09$	$0.76 \pm 0.03$
sqrt(M) weighting	<u><math>0.49 \pm 0.04</math></u>	<u><math>0.45 \pm 0.04</math></u>	<u><math>1.40 \pm 0.12</math></u>	$0.54 \pm 0.06$	$0.54 \pm 0.06$	$1.72 \pm 0.12$	$0.74 \pm 0.05$

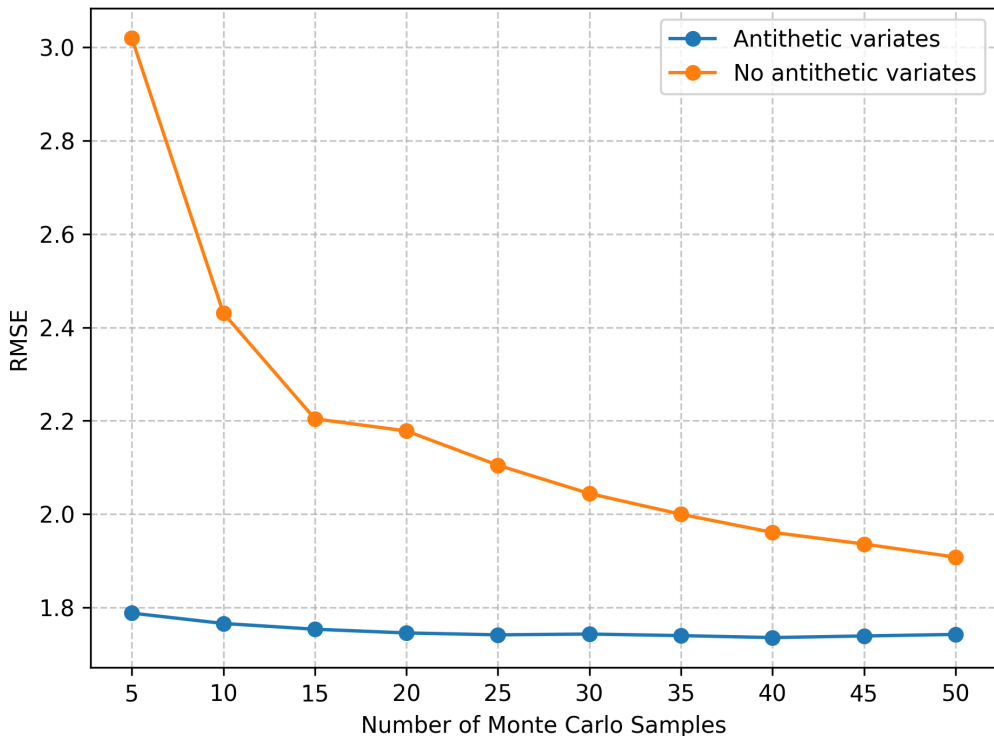


Figure 7. Overall RMSE vs. number of Monte Carlo samples evaluated using STAB-DDG parameters on the SKEMPIv2.0 test split.

## E. Additional details on the main text results

### E.1. Binding prediction accuracy on SKEMPIv2.0

#### E.1.1. COMPARISON TO BASELINE METHODS ON MORE METRICS

Here, we provide a more complete set of metrics to compare with other methods (Table 8).

#### E.1.2. RMSE BY AMINO ACID TYPE

We provide the average RMSE by mutant amino acid type in Table 9. We found that STAB-DDG achieved lower RMSEs for many bulky hydrophobic residues (PHE, TRP, TYR, MET).

Table 8. Evaluation of baseline  $\Delta\Delta G$  prediction methods and STAB-DDG on the test split of the SKEMPIv2.0 dataset. The best approach for each metric is in **bold** and per interface metrics for which the difference from the best is not statistically significant ( $P < 0.05$ ) are underlined. Statistical significance is determined by a paired, one-sided t-test to the best performing method. Standard errors for overall metrics are computed through cluster-bootstrapping.

Method	Per-Structure			Overall			
	Pearson	Spearman	RMSE	Pearson	Spearman	RMSE	AUROC
RDE-Net	0.30 $\pm$ 0.05	0.28 $\pm$ 0.05	1.53 $\pm$ 0.12	0.40 $\pm$ 0.05	0.40 $\pm$ 0.05	1.81 $\pm$ 0.10	0.63 $\pm$ 0.03
Surface-VQMAE	0.35 $\pm$ 0.05	0.33 $\pm$ 0.05	<u>1.48 <math>\pm</math> 0.11</u>	0.45 $\pm$ 0.04	0.44 $\pm$ 0.05	1.76 $\pm$ 0.09	0.65 $\pm$ 0.03
ProMIM	0.19 $\pm$ 0.06	0.15 $\pm$ 0.05	<u>1.57 <math>\pm</math> 0.12</u>	0.35 $\pm$ 0.06	0.35 $\pm$ 0.06	1.85 $\pm$ 0.11	0.60 $\pm$ 0.03
Prompt-DDG	0.32 $\pm$ 0.04	0.27 $\pm$ 0.04	<b>1.41 <math>\pm</math> 0.12</b>	0.33 $\pm$ 0.08	0.35 $\pm$ 0.07	1.81 $\pm$ 0.13	0.57 $\pm$ 0.05
DiffAffinity	0.26 $\pm$ 0.04	0.25 $\pm$ 0.04	1.55 $\pm$ 0.13	0.31 $\pm$ 0.05	0.33 $\pm$ 0.05	1.88 $\pm$ 0.11	0.64 $\pm$ 0.04
Flex ddG	<u>0.45 <math>\pm</math> 0.04</u>	<u>0.42 <math>\pm</math> 0.04</u>	<u>1.93 <math>\pm</math> 0.50</u>	0.22 $\pm$ 0.17	<b>0.54 <math>\pm</math> 0.05</b>	3.98 $\pm$ 1.65	<b>0.74 <math>\pm</math> 0.03</b>
PPIformer	0.20 $\pm$ 0.04	0.20 $\pm$ 0.04	1.51 $\pm$ 0.10	0.46 $\pm$ 0.07	0.42 $\pm$ 0.06	1.77 $\pm$ 0.09	0.71 $\pm$ 0.05
ProteinMPNN	0.14 $\pm$ 0.04	0.13 $\pm$ 0.04	—	0.18 $\pm$ 0.07	0.18 $\pm$ 0.06	—	0.55 $\pm$ 0.04
ESM-IF1	0.24 $\pm$ 0.04	0.22 $\pm$ 0.04	—	0.15 $\pm$ 0.05	0.23 $\pm$ 0.08	—	0.54 $\pm$ 0.05
StaB-ddG zero-shot	0.45 $\pm$ 0.04	0.43 $\pm$ 0.04	—	0.44 $\pm$ 0.07	0.43 $\pm$ 0.06	—	0.68 $\pm$ 0.04
Stability fine-tuned	0.45 $\pm$ 0.04	0.40 $\pm$ 0.04	1.69 $\pm$ 0.15	0.44 $\pm$ 0.06	0.45 $\pm$ 0.06	2.00 $\pm$ 0.12	0.70 $\pm$ 0.04
StaB-ddG	<b>0.49 <math>\pm</math> 0.04</b>	<b>0.45 <math>\pm</math> 0.04</b>	<b>1.41 <math>\pm</math> 0.12</b>	<b>0.53 <math>\pm</math> 0.06</b>	0.53 $\pm$ 0.05	<b>1.72 <math>\pm</math> 0.11</b>	0.73 $\pm$ 0.04

Table 9. RMSE for each mutant amino acid.

ALA	CYS	ASP	GLU	PHE	GLY	HIS	ILE	LYS	LEU	MET
1.32	3.19	2.96	1.96	0.94	1.33	2.06	1.90	1.61	1.67	1.58
ASN	PRO	GLN	ARG	SER	THR	VAL	TRP	TYR		
1.37	0.99	1.93	1.78	0.81	1.04	1.14	0.82	1.44		

### E.2. Yeast surface display case study details

**Estimation of a proxy for binding  $\Delta\Delta G$  from sequence counts.** We briefly summarize the procedure of estimating  $\Delta\Delta G$  from yeast surface display sorts described fully in [Cao et al. \(2022\)](#). A midpoint concentration ( $SC_{50}$ ) is estimated as a proxy for the binding dissociation constant  $K_D$  used to compute  $\Delta G_{\text{bind}}$ . The  $SC_{50,i}$  for sequence  $i$  is estimated using (Equation (1) [Cao et al. \(2022\)](#))

$$\text{Fraction\_collected}_i = \frac{\text{concentration}}{(\text{concentration} + SC_{50,i})}.$$

Here,  $\text{Fraction\_collected}_i$  is the fraction of bound sequences as determined by Fluorescence-Activated Cell Sorting (FACS) and Next Generation Sequencing (NGS). A critical assumption in this procedure is that expression level is constant across different sequences.

**Binding confounded by expression.** We found that our folding stability predictor was more accurate than our binding energy predictor at predicting binding energy on the yeast surface display dataset (Figure 4). We reasoned that this effect could be attributed to the sequence count readout from the yeast surface display experiment depended on both binding



affinity and expression, a quantity strongly correlated with folding stability (Cao et al., 2022). We validated this hypothesis by experimenting with predictors of the form

$$b_{\theta}(s_{A:B}) = f_{\theta}(s_{A:B}) - \beta[f_{\theta}(s_A) + f_{\theta}(s_B)].$$

The case that  $\beta = 0$  corresponds to the “complex” only predictions. And the case that  $\beta = 1$  corresponds to STAB-DDG parameterization, where  $\beta$  is a constant. We found that, indeed, setting  $\beta = 0.65$  improved performance of all predictors (Figure 8).

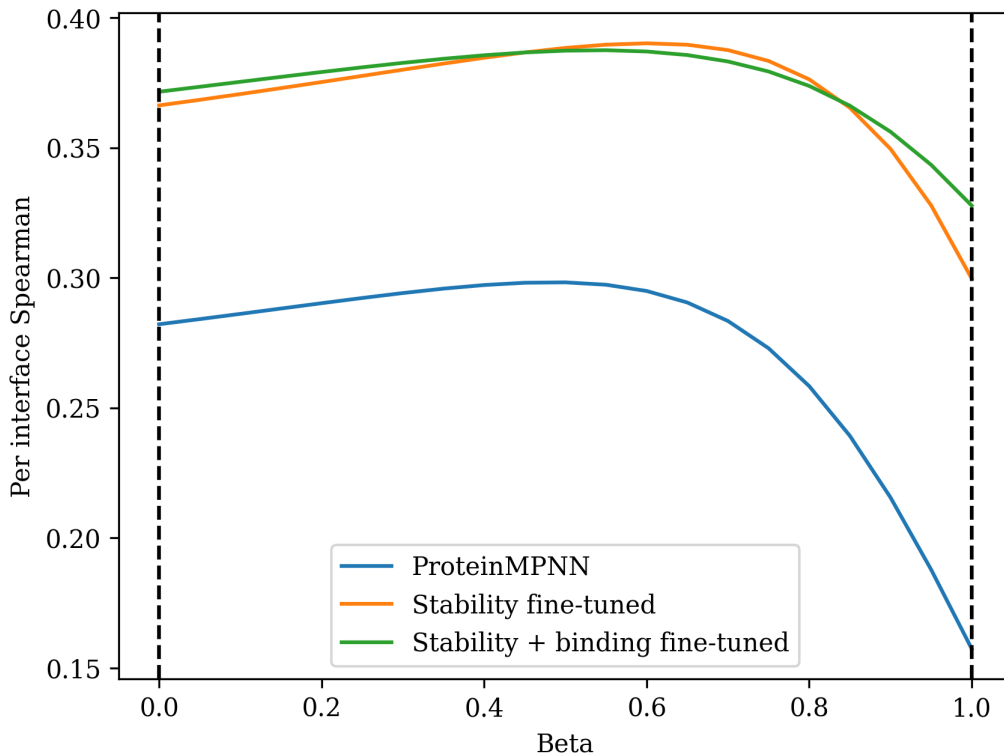


Figure 8. Spearman vs. different values of  $\beta$  on the yeast surface display dataset.  $\beta = 0$  corresponds to the folding energy predictor  $\Delta f_{\theta}$ , and  $\beta = 1$  corresponds to the binding energy predictor  $\Delta b_{\theta}$ .

Table 10. Evaluation of  $\Delta\Delta G$  prediction on yeast surface display dataset.

Method	Pearson	Per-Structure Spearman	RMSE	Overall			
				Pearson	Spearman	RMSE	AUROC
StaB-ddG zero-shot	$0.157 \pm 0.020$	$0.094 \pm 0.015$	$1.43 \pm 0.08$	0.16	0.10	1.45	0.54
StaB-ddG zero-shot complex	$0.282 \pm 0.023$	$0.274 \pm 0.025$	$3.02 \pm 0.09$	0.25	0.26	3.08	0.61
Stability fine-tuned	$0.300 \pm 0.022$	$0.268 \pm 0.021$	$1.24 \pm 0.10$	0.28	0.26	1.30	0.61
Stability fine-tuned complex	$0.366 \pm 0.030$	$0.314 \pm 0.030$	$1.26 \pm 0.07$	0.31	0.29	1.26	0.62
StaB-ddG	$0.328 \pm 0.025$	$0.296 \pm 0.026$	$1.21 \pm 0.09$	0.32	0.28	1.25	0.62
StaB-ddG complex	$0.372 \pm 0.030$	$0.323 \pm 0.031$	$1.35 \pm 0.06$	0.32	0.30	1.35	0.63

### E.3. Comparison to ThermoMPNN

In this section we compare the performance of STAB-DDG on folding stability prediction with ThermoMPNN, a state-of-the-art method for predicting the effects of single mutations on protein stability. ThermoMPNN is based on ProteinMPNN and introduces an additional attention-based neural network for fine-tuning on the Megascap dataset. We use the same training split as ThermoMPNN to fine-tune STAB-DDG. However, as STAB-DDG naturally generalizes to mutants with

multiple mutations, we include such mutants for structures in the training set. We evaluate STAB-DDG on the same test set as ThermoMPNN (Table 11). We report the metrics computed on the test set as a whole, rather than averaging performance across domains. In addition to ThermoMPNN, we include the next best two baselines reported by Dieckhaus et al. (2024) for reference. STAB-DDG achieves performance not much below that of ThermoMPNN and outperforms the next best baseline (Dieckhaus et al., 2024). We also assess the performance on multiple mutations for our method (Table 12). We found that though our method performed comparably to ThermoMPNN on single mutations, our stability predictor achieved significantly lower accuracy on multiple mutations, presumably due to the limited amount of multiple mutation data.

Table 11. Performance on Megascale test set (single mutations).

METHOD	PEARSON	SPEARMAN	RMSE
THERMOMPNN	0.75	0.73	0.71
STABILITY FINE-TUNED (OURS)	0.71	0.69	0.77
RASP	0.71	0.67	1.08
PROSTATA	0.64	0.59	0.83

Table 12. Performance on Megascale test set (multiple mutations).

METHOD	PEARSON	SPEARMAN	RMSE
STABILITY FINE-TUNED (OURS)	0.38	0.42	1.41